Journal of Applied Fluid Mechanics, Vol. 17, No. 2, pp. 322-336, 2024.
Available online at www.jafmonline.net, ISSN 1735-3572, EISSN 1735-3645.
https://doi.org/10.47176/jafm.17.02.2095

An Analysis of the Minimum Pressure Coefficient Criterion Applied to the Axial-flow Pump Design – A Case Study for a Circulating Water Channel

R. V. Correia Ramalho[1†], A. L. Amarante Mesquita[1] and N. Manzanares Filho[2]

[1] *Laboratory of Fluid Dynamic and Particulate (FluidPar), Federal University of Pará, Tucuruí, Pará, 68455-901, Brazil*
[2] *Mechanical Engineering Institute, Federal University of Itajuba, Itajuba, Minas Gerais, 37500-903, Brazil*

†*Corresponding Author Email: rodolfo.ramalho@tucurui.ufpa.br*

ABSTRACT

An analysis of the minimum pressure coefficient on the suction side of the axial-flow pump blades is presented as a design criterion. A Matlab code is used to improve the computer aided design process efficiency and quality. X-Foil software determines the blade profiles' lift and drag coefficients, and a computational fluid dynamics model is applied to certify the pump efficiency. The model is validated from the available experimental data in the literature. The finite volume method is used through the commercial software Ansys CFX, in order to solve the model equations. A case study is presented to design the axial-flow pump for a large circulating water channel that will be used to test ships, naval structures, and hydrokinetic turbines. Particular attention is given to the pump cavitation conditions. The model evaluates the minimum pressure coefficient criterion and pressure coefficient distribution on the blade span, showing satisfactory performance for the pump at the design point and at variable speed.

Article History

Received June 17, 2023
Revised August 29, 2023
Accepted September 28, 2023
Available online December 4, 2023

Keywords:

Turbomachinery
CFD
Performance optimization
CFX
Finite Volume Method

1. INTRODUCTION

In the Amazon, most of the population lives along the thousands of rivers in the world's largest watershed. For these people, the main means of transport is the boat. In this context, the Brazilian government created a program to develop special boat to meet the need of children to reach schools (Amarante Mesquita et al., 2015). For this development, Circulating Water Channels (CWCs) are key facilities, which can also be employed for other studies such as naval structures (Gucheng et al., 2021) and hydrokinetic turbine research (Martinez et al., 2020; Guo et al., 2020) .

To minimize model scale effects, large CWCs are needed; therefore, large axial-flow pumps are required to promote water flow. This type of pump is not easily available in the market, and special designs are needed to match the required CWC operational conditions (Ahn et al., 2008; Watanabe et al., 2009; Hosono et al., 2015). In addition, few studies are found in the literature on the design of large axial-flow pumps (Choi et al., 2021).

To promote the development of these scholar boats and hydrokinetic turbine development (Holanda et al., 2017; Silva et al., 2017), a large CWC was designed at the Federal University of Pará, Brazil. For an initial configuration of a quasi-horizontal CWC, two axial-flow pumps were specified, and due to the difficulty of the market, in both, availability and high prices, a decision was made to design and manufacture the pumps.

Information on the axial-flow pump design has been available in the literature since the classical publication (Stepanoff, 1957) to the present (Nguyen et al., 2023). However, the requirement for a reliable design is a combination of basic global empirical criteria, fundamental turbomachinery formulation, a design criterion to define the rotor geometry, and a modern tool for complex flow analysis, such as CFD modelling (Denton, 2010; Pinto et al., 2017; Tyacke et al., 2019). In this context, this work details the application of the minimum pressure coefficient criterion to the design of axial-flow pumps. The case study is the pump designed for a large CWC, including a CFD flow study to certify the required flow and head, with high efficiency and free cavitation behavior.

The typical approaches employed in the design of axial flow pump blades include the lift method, circular arc method, and singularity distribution method.

Nomenclature

c	absolute velocity	w	relative velocity
C_D	drag coefficient, related to the mean velocity	w_3	inlet relative velocity
C_L	lift coefficient	w_6	outlet relative velocity
$Cpmin$	minimum suction pressure coefficient	w_∞	mean relative velocity
C_p	pressure coefficient		
C_r	radial velocity component	**Greek Letters**	
C_m	meridian velocity		
D	runner diameter	Δp_o	stagnation pressure loss
Y	specific energy		
H	head	Δc_u	difference between the tangential velocity components
l	chord of profile	α	angle of attack in relation to w∞
n	rotational speed	β	construction angle
n_q	specific speed	β_3	inlet flow angle
N_p	number of blades	β_6	outlet flow angle
p	static pressure on the blade profile	β_∞	mean angle of flow velocity
P	power	$\Delta\beta$	cascade deflection angle
P_h	hydraulic power	ΔW_u	difference between the tangential velocity components
P_u	shaft power	δ	specific diameter
p_o	reference pressure	λ	cascade solidity
p_3	inlet static pressure	η	pump efficiency
p_4	outlet static pressure	η_h	pump hydraulic efficiency
Q	flow rate	ν	diameter relation
R	radius	ρ	fluid density
t	cascade pitch	σ	specific speed
T	torque	σ_t	Thoma coefficient
u	tangential velocity	ω	angular velocity
u_e	tangential velocity at blade tip	ψ	pressure coefficient number

In tandem with the rapid advancement of computer technology, optimization design techniques based on Computational Fluid Dynamics (CFD) have undergone swift development. By utilizing numerical calculations derived from axial flow pump analysis, adjustments are made to the geometric parameters of the blades. This leads to an enhancement in the pump's internal flow pattern, effectively preventing the occurrence of undesirable phenomena such as vortices, backflow, and secondary flows (Shi, 2016).

This work aims to use the advances in CFD technology to increase the knowledge base about the Cpmin design criterion in large axial flow pumps, considering that recently this method has been used for the design of small axial turbines (Haghighi et al., 2019; Zhang et al., 2022)

Some studies have demonstrated the validity of using the minimum pressure coefficient (*Cpmin*) criterion in cascade selection for the design of axial turbomachinery. Scholz (1965) initially used the minimum pressure coefficient as a loading criterion in isolated profiles. Later, Fernandes (1973) extended the applicability of the minimum pressure coefficient criterion to cascade profiles, designing and conducting experimental studies on a series of axial-flow pumps using Göttingen profiles. The minimum pressure coefficient criterion was also evaluated in axial-flow fan design as an aerodynamic loading criterion for selecting cascades with minimal loss (Amarante Mesquita et al., 1999). Cruz et al. (2008) also proposed and successfully tested the design of low head axial-flow hydraulic turbines, and their methodology was well accepted in the literature (Haghighi et al., 2019; Zhang et al., 2022). Sutikno and Adam (2011) confirmed the use of the minimum pressure coefficient as an efficient design criterion for very low head axial-flow hydraulic turbines through experimental tests and numerical simulation. The results obtained by Muis et al. (2015) through a 3D CFD numerical study also showed very good performance for very low-head turbines designed using the minimum pressure coefficient criterion. Haghighi et al. (2019) also verified a strong influence of the pressure coefficient on the performance of low-head axial turbines using a multiphase CFD model. However, this approach needed to be applied together with cavitation analysis to assure reliable operation (Dönmez et al., 2023; Wang et al., 2023).

In this study, the Ansys TurboGrid software package, specific for working with turbomachinery geometries, was used to generate the mesh of the CFD simulation domain. The mesh's structure is defined as automatic topology and meshing (ATM), employing a single round-round symmetric approach. This choice of topology generates an excellent grid, eliminating the need for manual adjustment of control points. This technique automatically produces an optimized topology grid by leveraging blade characteristics at various points along the blade's length. As a result, it achieves a top-notch mesh quality with minimal exertion (Ansys, 2015).

The CFD model was implemented by the Ansys CFX package. The characteristic curves of the pump were

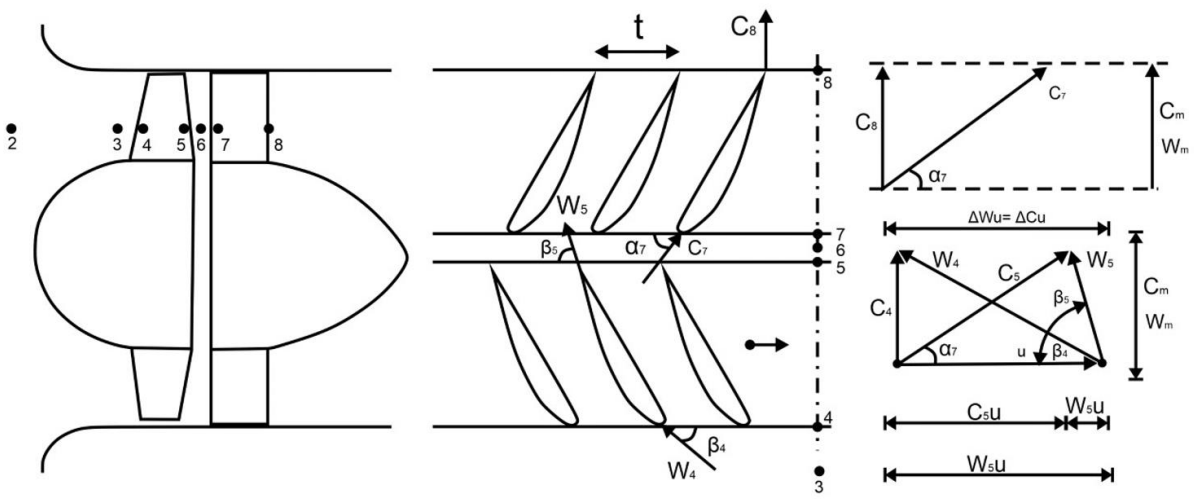

Fig. 1 Axial-flow pump radial section and velocity vectors

obtained using the finite volume method to solve the Reynolds-averaged Navier–Stokes (RANS) equations, and the k-ω SST turbulence model was used since it was the most widely recommended when there was flow separation (Menter, 1993; Al-Obaidi, 2019). The results obtained by our CFD model were compared and validated with experimental characteristic curves obtained by Fernandes (1973). Our CFD model was used to obtain the performance curves of the axial-flow pump designed to promote the flow for the CWC of the case study. Our results demonstrated the validity of the minimum pressure coefficient as a performance criterion for axial-flow pump design.

2. DESIGN METHOD FOR AXIAL FLOW PUMPS

2.1 Empirical Global Design Parameters

The first step of the pump design is the definition of the main dimensions of the rotor. The procedure is based on cascade theory, as proposed by Wu (1952). For a generalized analysis, the parameters are presented in dimensionless form. A turbomachine is characterized by its specific speed, nq, which determines the type and basic shape of the rotor. According to Pfleiderer and Petermann (1979), the specific speed is usually given by Eq. (1).

$$n_q = \frac{nQ^{1/2}}{(gH)^{3/4}} \tag{1}$$

The head coefficient ψ is used together with the specific speed to obtain the basic geometric parameters of the rotor and is presented in Eq. (2).

$$\psi = \frac{2(gH)}{u_e^2} \tag{2}$$

In our work, for the initial stipulation of the hydraulic efficiency of the machine, the Cordier diagram was used as a function of two dimensionless coefficients, the specific speed σ and the specific diameter δ, defined by Eq. (3,4) (Castegnaro, 2018).

$$\sigma = 2.108\, n_q \tag{3}$$

$$\delta = \frac{1.054(Y^{0.25})}{Q^{0.5}} D \tag{4}$$

The main dimensions of an axial rotor are the ratio between the inner diameter and the outer diameter υ and the number of rotor blades, Np. The impeller and diffuser of axial-flow pumps can consist of vanes whose profiles are derived from airfoils. Thus, it can be ensured that the flow required is performed with the highest efficiency possible. High-speed propeller pumps are equipped with just two impeller blades; with decreasing specific speed nq, the number of blades increases to approximately eight at n_q = 0.5. Thus, the number of blades selected for our case was 3 (Jaberg, 1999).

2.2 Fundamental Design Equations

The rotor blade is divided into some parallel planes from hub to tip, and the calculation is performed at nine unfolded cylindrical sections (cascades). In axial propeller pumps, the flow approximately moves along a coaxial cylindrical section. The handled fluid enters the impeller in the axial direction and leaves it, as illustrated in Fig. 1, with angular momentum and thus a higher absolute and lower relative velocity. In Fig. 1 the flow goes from point 1 to point 8 with point 4 and 5 representing the blade leading edge and trailing edge, respectively.

By a second redirection in the axial direction in the diffuser with a consequent further deceleration, it also contributes to pressure generation (Jaberg, 1999).

The pump stator is usually built via circular arc profiles with constant thickness for all sections. The methodology of Srinivasan (2008) was used to design these profiles, consisting of using Howell's diagram to obtain the solidity based on the entry and exit angles of the hub section. For the same blade sections selected for the rotor, the entrance angle of the stator vane cascades is used.

2.3 Euler's Equation and Fundamental Design Equations

In general, the analysis of flow through two-dimensional pump cascades considers the radial velocity component to be null, with the current surfaces remaining cylindrical and parallel to the rotation axis. This condition is possible if the meridian velocity remains constant. Based on this condition, Euler's Equation (Eq. 5) can then

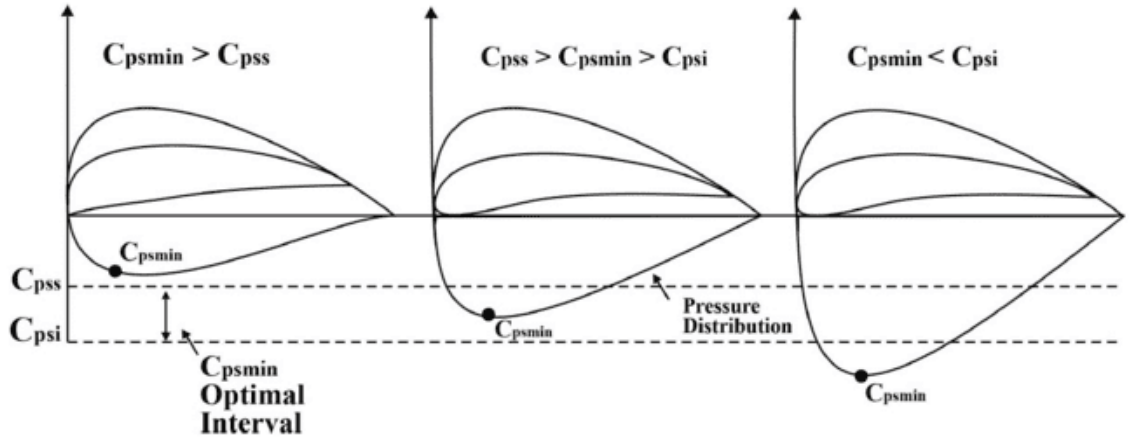

Fig. 2 Minimum pressure coefficient criterion

be applied to the pump design to determine the circumferential velocity components necessary to generate the required pressure.

$$Y_{blade} = \frac{gH}{n_h} = \frac{u(c_{u_5} - c_{u_4})}{\eta_h} = \frac{u.\Delta c_u}{\eta_h} \quad (5)$$

The cascade moves with velocity u. The cascade deflection angle is defined as $\Delta\beta = \beta_6 - \beta_3$. The angles β_3 and β_6 define the direction of the inlet w_3 and outlet w_6 flow velocities taken about the axial direction, respectively. Observing the geometric relations, the following relationship between the angles of the flow and the cascade is verified: $\beta = \beta_\infty + \alpha$, where β is the stagger angle, β_∞ is the mean angle that defines the direction of the mean flow velocity, and α is the angle of attack taken about the w_∞ velocity.

The flow is considered to be two-dimensional, incompressible, isothermal, and in a steady-state condition. Applying the momentum equation in both axial and tangential directions, the following expressions (Eq. 6,7) are obtained:

$$c_l \cdot \lambda = -\zeta_v \cos^2 \beta_\infty \cdot \sin \beta_\infty + 2 \cdot \delta_u \cdot cos\ \beta_\infty \quad (6)$$

$$c_d \cdot \lambda = \zeta_v \cos^3 \beta_\infty \quad (7)$$

Where c_l is the lift coefficient, c_d is the drag coefficient, β_∞ is the angle between the mean velocity and the axial direction, w_∞ is defined by Eq. (8), λ is the cascade solidity and the relationship between the blade chord l and the cascade pitch t (distance between a blade and another adjacent blade), and ζ_v is the dimensionless loss coefficient of the cascade defined by Eq. (9,10).

$$\overrightarrow{w_\infty} = \frac{\overrightarrow{w_3} + \overrightarrow{w_6}}{2} \quad (8)$$

$$\zeta_v = \frac{\Delta p_o}{\frac{1}{2}\rho w_a^2} \quad (9)$$

$$\Delta p_o = \left(p_3 + \frac{1}{2}\rho w_3^2\right) - \left(p_6 + \frac{1}{2}\rho w_6^2\right) \quad (10)$$

Where Δ_{po} represents the global loss of the stagnation pressure through the cascade and p_3 and p_6 are the inlet and outlet static pressures, respectively. For inviscid flow, $C_D = 0$; consequently, $\zeta_v = 0$, and Eq. (6) reduces to Eq. (11).

$$c_l \cdot \lambda = \frac{2\Delta c_u}{w_\infty} \quad (11)$$

Equation (11) is the classical relationship used in turbomachinery design, which can also be derived from the Kutta-Joukowsky theorem. The term $c_l \cdot \lambda$ is associated with the constructive characteristics of the turbomachinery, which is defined by the cascade that can reproduce the characteristics of the desired flow. The term $\frac{2\Delta c_u}{w_\infty}$ is associated with the characteristics of the flow.

2.4 Minimum Pressure Coefficient Criterion

The minimum pressure coefficient, *Cpmin*, is the minimum value of the pressure coefficient pertaining to the suction side of the blade profile. This parameter is characteristic of an axial flow turbomachine since it considers not only the hydrodynamic parameters but also the influence of the geometric parameters of the cascade, thus having a more generalized meaning than the lift coefficient. In the literature (Fernandes, 1973), the following limitation Eq. (12) is indicated as a criterion for dimensioning the cascade geometry:

$$C_{pmin} = 1{,}60\ to\ 1{,}80 \quad (12)$$

This limitation applies to the sections of the blade close to the rotor hub. Figure 2 illustrates the minimum pressure coefficient criterion, where C_{psi} and C_{pss} represent the lower and upper limits of the pressure coefficient, respectively.

According to the work of Scholz (1965), values greater than -1.6 (C_{pss}) indicate limit conditions with a tendency towards efficiency loss due to the considerable friction observed in this situation. On the other hand, values lower than -1.8 (C_{psi}) indicate a tendency towards a reduction in head and efficiency due to the flow separation verified in these situations.

2.5 Cavitation Analysis

Xie et al. (2019) and Ye et al. (2022) investigated cavitation in axial-flow pumps operating at variable speeds, and their results not only showed the impacts of cavitation on the performance of axial pumps but also provided a reference for the study of the cavitation mechanism for axial flow pumps using CFD. The axial-

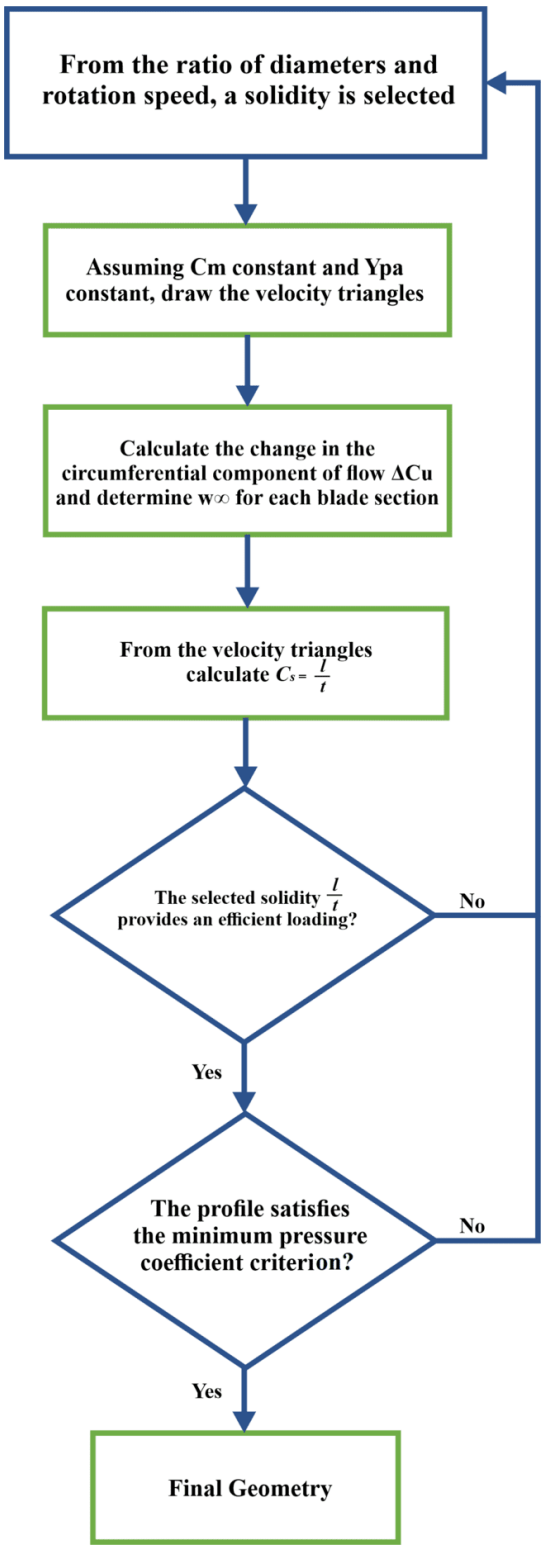

Fig. 3 Design strategy

flow pump's susceptibility to cavitation is heightened in comparison to other pump types, owing to its attributes of high flow and low head. Prolonged cavitation will detrimentally impact the impeller's energy conversion, resulting in diminished hydraulic efficiency of the pump system. Furthermore, this phenomenon will initiate vibrations and noise within the pump apparatus, potentially leading to cavitation-induced harm to the axial-flow pump's blades. Such damage could significantly jeopardize the operational safety of the entire pump station.

To predict the occurrence of this phenomenon already in the machine design stage, the Thoma coefficient, or cavitation coefficient, presented in Eq. (13) was used.

$$\sigma_t = \frac{p_o - p_v}{\frac{1}{2}\rho w_\infty^2} \tag{13}$$

Silva et al. (2017) proposed optimizing the design of the chord of hydrokinetic turbine profiles that avoids cavitation using the Thoma coefficient and treating the reference pressure as the sum of the atmospheric pressure (atm) with the local water column h as a function of the radial position of each blade section. Cavitation occurs if the minimum pressure coefficient of a given blade section is less than the Thoma number of the same section, according to Eq. (14).

$$\sigma_t + Cpmin \geq 0 \tag{14}$$

2.6 Design Strategy

Hydrodynamic parameters, such as lift, drag, and minimum pressure coefficient, were calculated using the free software X-Foil, which uses the panel method, in conjunction with mathematical formulation, to calculate pressure variations around the surfaces of the profiles. The software also calculates the viscous/non-viscous interactions by solving the panel method and boundary layer equations simultaneously (Drela, 1989). For each section, the following strategy (Fig. 3) was used to select the profile geometry.

Considering the available space, the typical dimensions of existing school boats, the estimated maximum speed for the boats, and the characteristics intended for the tests to be carried out, the channel was dimensioned based on existing methodologies in the literature (Stephen, 1971; Assi et al., 2005; Grinberg et al., 2011). The main dimensions and pump configuration are shown in Fig. 4.

The parameters for defining the operating point of the pump are shown in Table 1, where the head was estimated from a simplified calculation of pressure loss in the channel and considering the difference in level between the test section and the return channel section.

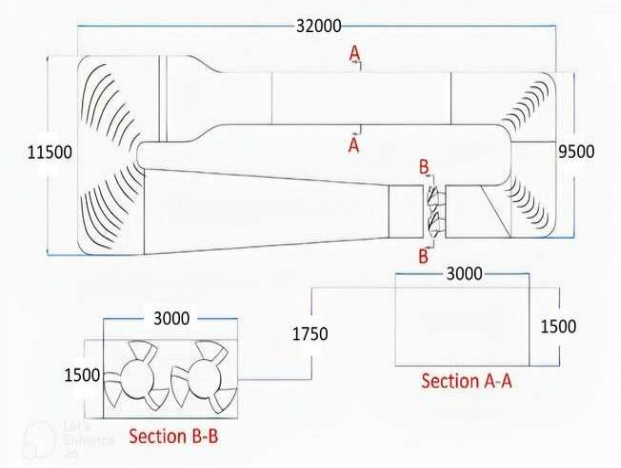

Fig. 4 Main dimensions of the water recirculating channel (in mm)

Table 1 Water channel pump operating parameters

Parameter	Value
Flow Rate (m³/s)	6.75
Head (m)	2.5
Rotation Speed (rpm)	200
Test section flow speed (m/s)	3.00
Diameter (mm)	1475.00
Specific Energy (J/kg)	24.52
ψ(-)	0.21
n_q (-)	0.79
Blade Number	3
Power (kW)	165

3. CFD MODELLING

3.1 Numerical Methods

The commercial CFX code, which solved the Navier–Stokes 3D equations in its conservative form, was used as the basis for the flow solution. This code is an element-based finite volume method (EbFVM) solver with a cell vertex formulation and is used for the resolution of the algebraic equations inside the simulation domain through spatial discretization. The governing equations along with boundary conditions were solved using a second order up-winding scheme (high resolution).

A moving reference frame (MRF) was used since this case had domains that were rotating relative to one another. MRF is based on general grid interface (GGI) technology, which allows rotor/stator interaction in the investigation of turbomachinery in Ansys-CFX. In the GGI, a control surface approach was used to connect across the interface or periodic condition through an intersection algorithm.

The simulation domain included the space between the pump inlet and outlet, hub, and shroud region (Fig. 5). The flow was assumed to be turbulent and in a steady-state condition. The k-ω SST turbulence model was used to simulate the fluid flow since it was the most recommended model when there was flow separation. The domain was selected to allow the flow to arrive completely developed at the pump inlet and the outlet to be far enough away from the pump such that there were no fluid turn problems.

Governing Equations

The main equations used in the present study are the continuity, momentum, and Navier Stokes equations. (Eq. 15-17), respectively.

$$\frac{\partial \rho}{\partial t} + \nabla \cdot (\rho u) = 0 \tag{15}$$

$$\partial(\rho u)\partial t + \nabla \cdot (\rho u \times u) = -\nabla p + \nabla \cdot \tau + F \tag{16}$$

$$\rho\left(\frac{\partial \overline{u}}{\partial t} + \overline{u} \cdot \nabla \overline{u}\right) = \rho g - \nabla p + \mu \nabla^2 \overline{u} \tag{17}$$

where F is the sum of body forces and τ is the stress tensor (Eq. 18).

$$\tau = \mu_t(\nabla u + (\nabla u)T - \frac{2}{3}\delta \nabla \cdot u \tag{18}$$

where μ_t is the effective viscosity accounting for the turbulence through a turbulence model, such as the *k-ε* or $k - \omega\ SST$.

Turbulence Closure

Various turbulence models are available to capture the turbulence behavior of the flow. There is consensus on the need for two representative kinematic quantities for the correct determination of turbulence. Therefore, the model used in this work is a two-equation model, with its reliability already established in the literature (Wilcox, 2006).

The k-ω shear stress transport (SST) turbulence model is a widely used turbulence model in computational fluid dynamics (CFD) simulations. It is an extension of the k-ω model that improves its performance in regions of flow with adverse pressure gradients, separation, and reattachment. The k-ω SST model solves two transport

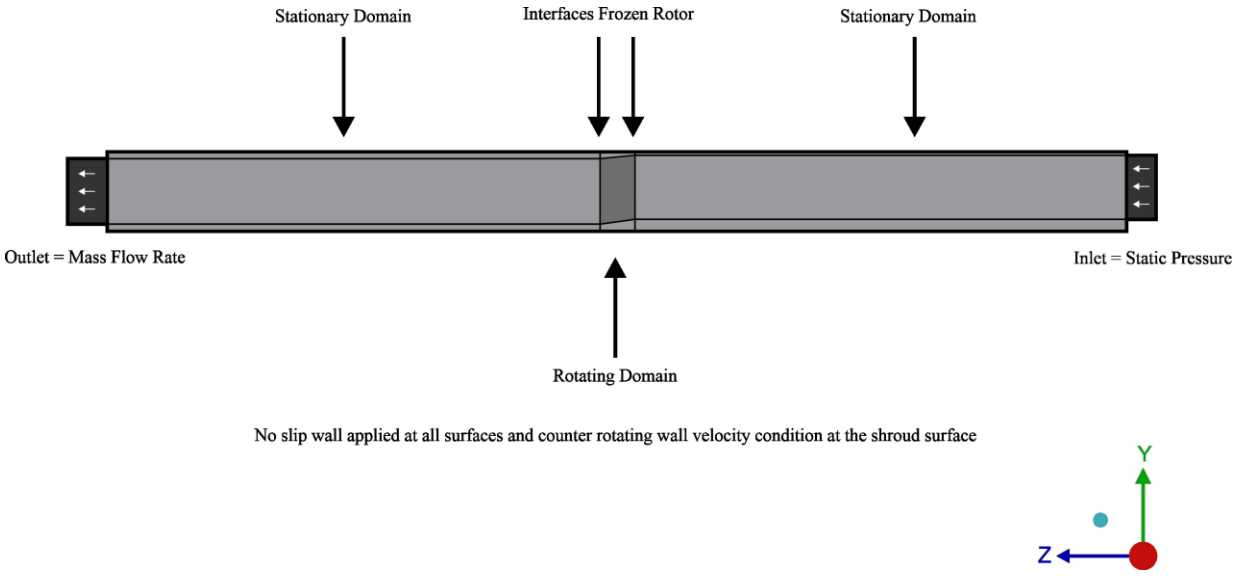

Fig. 5 Simulation domain

Table 2 Boundary conditions

Boundary	Setting	Value/Method
Inlet	Mass Flow Rate	39.88 kg/s
Outlet	Static Pressure	17500 Pa
Rotor	Wall	Soft Wall
Shroud	Wall	Counter Rotating
Hub	Wall	Soft Wall
Interface rotor/inlet	Interface	Frozen Rotor

equations for the turbulent kinetic energy (k) and the specific dissipation rate (ω) of the turbulence. The model also includes an additional transport equation for the eddy viscosity (ν_t), which is used to close the system of equations.

The k-ω SST model created by Menter (1993) assumes that the turbulence in the flow can be divided into two regions: a viscous sublayer near the wall and a turbulent core region away from the wall. In the viscous sublayer, the model uses a modified version of the k-ω model to account for the effects of wall-bounded turbulence. In the turbulent core region, the model switches to a shear stress transport (SST) model, providing improved performance in regions of adverse pressure gradients and separation.

The SST model assumes that turbulence can be decomposed into two components: turbulent kinetic energy and Reynolds shear stress. The model includes additional transport equations for the turbulent viscosity and the Reynolds shear stress to account for the effects of the anisotropic nature of turbulence in the flow.

The k-ω SST model has been shown to provide accurate predictions of turbulent flow in a wide range of applications, including flows with strong pressure gradients, separation, and reattachment. It is widely used in the aerospace, automotive, and energy industries for CFD simulations of complex fluid flow problems (Menter et al., 2020).

Boundary Conditions

Appropriate boundary conditions need to be defined for each boundary of the computational domain to represent the physical conditions at those boundaries. Standard wall conditions were considered for the shroud and propeller walls. The parameters considered in the analysis are listed in Table 2.

3.2 Numerical Solution

Numerical Procedures

For the generation of the domain mesh, the ANSYS mesh generation package Turbogrid was used. In this package, the domain was discretized with an unstructured mesh. The first layer of the mesh was carefully refined to ensure good resolution in the boundary layer region (y+ <= 1), and a division of at least 25 elements was defined at the leading and trailing edges of the blades in the span direction and 100 elements in the flow direction. The minimum number of cells was defined as 10 cells between the blade tip and the pump casing to ensure good refinement in this region, which had high velocity gradients. In addition, the mesh quality factors issued by the program were also used as a mesh analysis criterion. Meshes obtained following these recommendations are shown in Figs. 6-8.

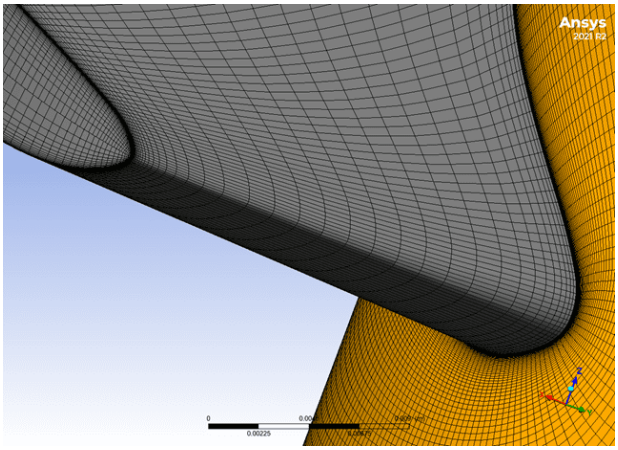

Fig. 6 Leading edge mesh

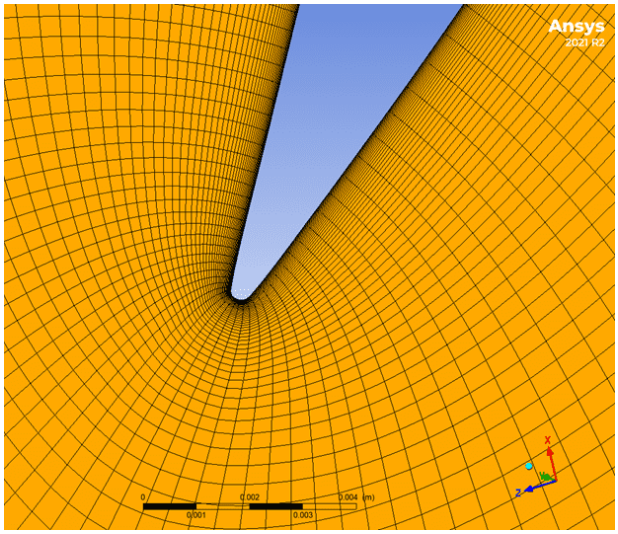

Fig. 7 Trailing edge mesh

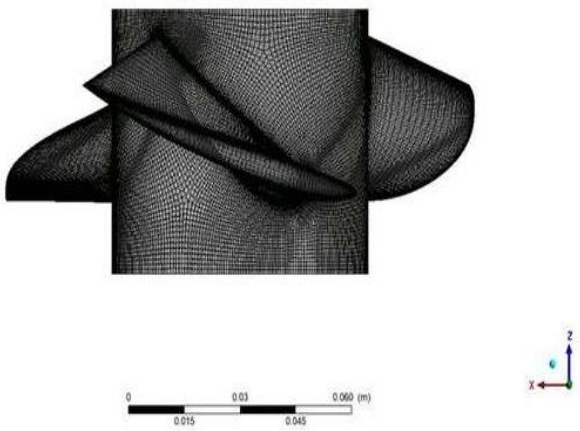

Fig. 8 Rotor tridimensional mesh

Table 3 Mesh convergence

Mesh	Nº of elements	Efficiency	Head (m)
Experimental	-	50%	3.691
Mesh 1	$2.41 \cdot 10^6$	59%	4.62
Mesh 2	$3.03 \cdot 10^6$	53%	4.13
Mesh 3	$3.16 \cdot 10^6$	52%	4.09
Mesh 4	$3.52 \cdot 10^6$	52.1%	3.91
Mesh 5	$4.11 \cdot 10^6$	52.09	3.89

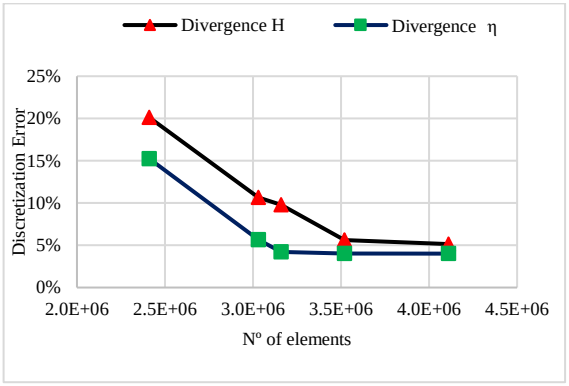

Fig. 9 Mesh independence test

Mesh Convergence

As is natural in any numerical analysis, a mesh convergence study was necessary to determine the dependence between the results and the mesh. Therefore, in this work, two criteria were imposed for the study of the mesh. First, all meshes needed to obey a minimum criterion of skewness, aspect ratio and orthogonality. Second, the selection of the mesh was made using a grid convergence index (GCI), which is the change in the value of a certain variable in response to a different grid spacing, and a value of 5% is set as the mesh selection criterion, using the highest value found for both parameters (head and efficiency). Thus, an intermediate mesh (Mesh 4) was selected to ensure both the robustness of the results and a reasonable computation time. Below is the table with the meshes used and the mesh convergence. (Table 3 and Fig. 9).

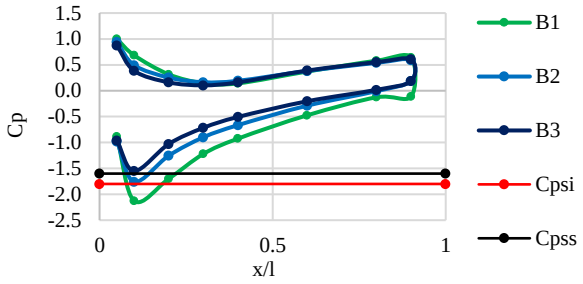

Fig. 10 Pressure coefficient of the experimental pump

Table 4 Experimental study pump parameters

n_q	Pump	*Cpmin*	λ (l/t)	β (degree)	C_s
0.6	B1	-2.13	0.6	38.6	1.659
	B2	-1.76	0.8	36.2	1.244
	B3	-1.55	0.95	35.0	1.082

CFD Validation

Axial-Flow Pump Experiment

For the analysis of the flow in the cascade and, therefore, application of the criterion of the minimum pressure coefficient, Fernandes (1973) used the method of singularities, which consisted of the representation of each profile by a distribution of sources, sinks, and vortices. Using the Schlichting and Truckenbrodt (1959) solution, three values of the minimum pressure coefficient were tested, with only one being within the criterion range. The main pump parameters are shown in Table 4. Figure 10 shows the calculated pressure coefficient distribution at the hub profile for each pump.

To obtain the main geometric parameters of the machines, Cordier diagrams and cascade theory were used, as shown in Section 2 of this work. For the design of the pump, the blades were divided into 3 sections. For the pumps, 3 profiles from the Göttingen family were used for each geometry. The pumps are illustrated in Fig. 11.

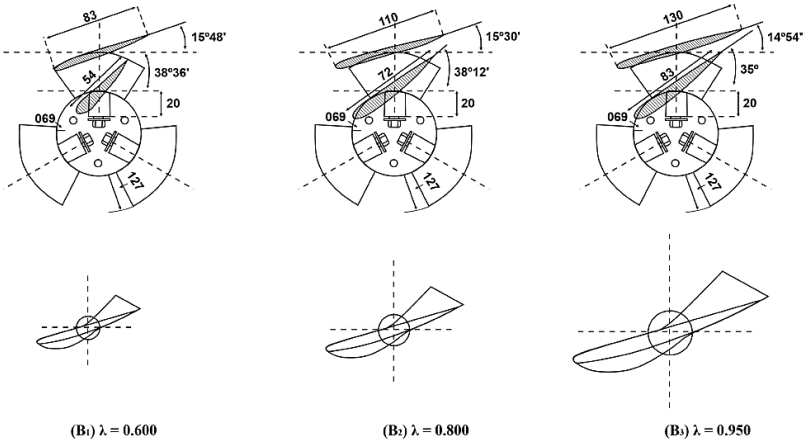

nq = 0.600
Ψ = 0.195
ν = 0.543

Fig. 11 Pump geometry

Validation Results

Using Mesh 4, the results were generated with the aid of the ANSYS postprocessing tool CFX-post, as shown in Figs. 12-14. As observed, for the design flow Qo, the pressure coefficient value was very close to the design flow for the entire blade extension. However, when the pump began to operate under off-design conditions, the value of the coefficient began to vary, leading to considerable efficiency losses, as shown by the performance curves in Figs. 15, 16.

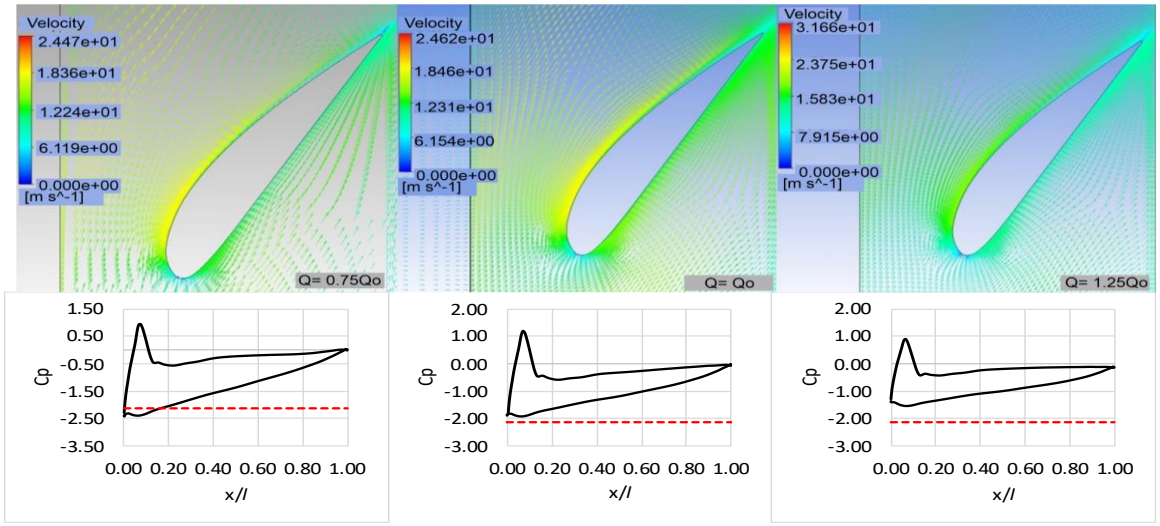

Fig. 12 Velocity vectors and pressure distribution around the blade hub

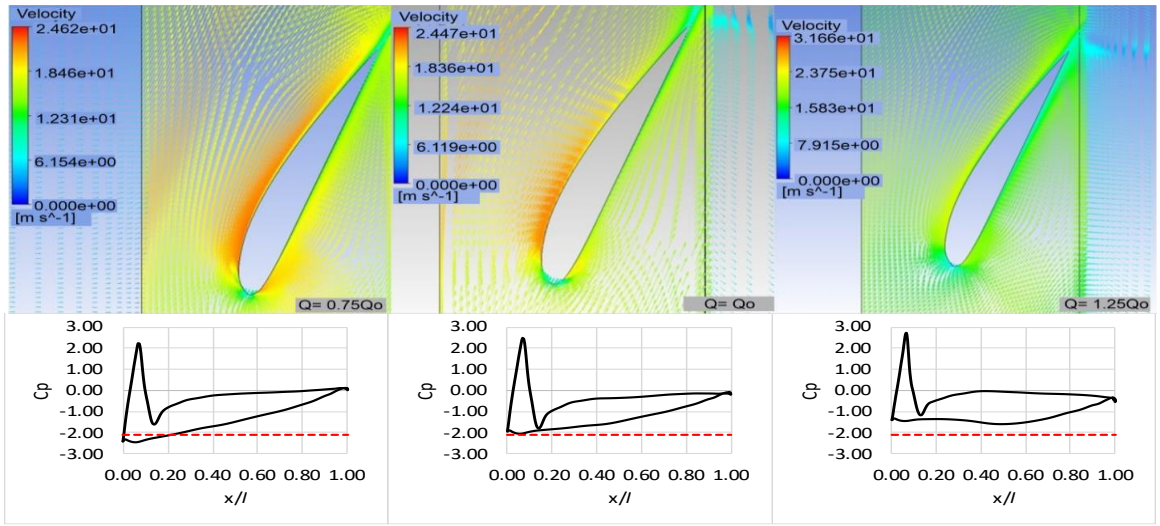

Fig. 13 Velocity vectors and pressure distribution around the blade mid span

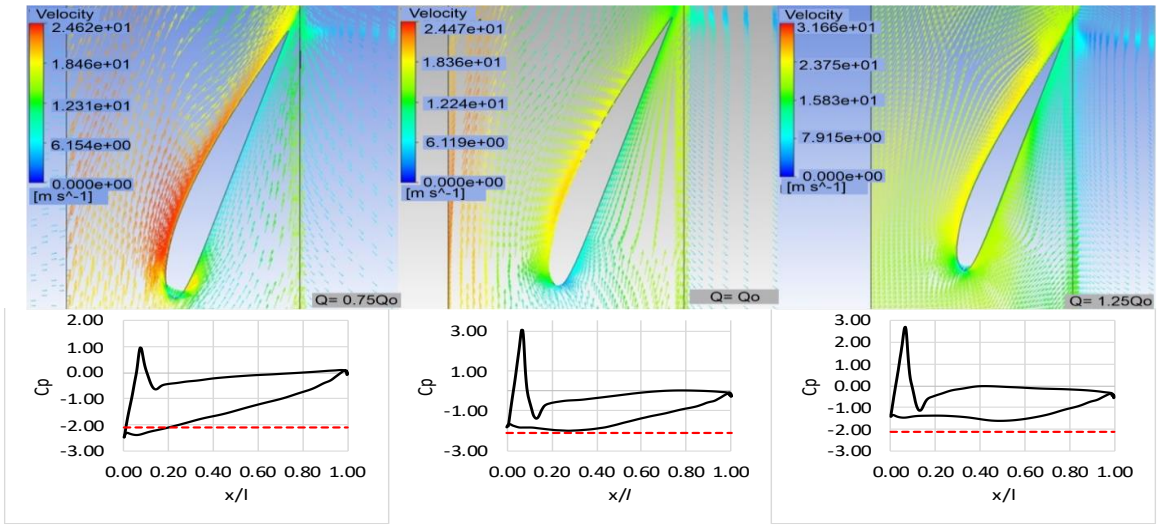

Fig. 14 Velocity vectors and pressure distribution around the blade tip

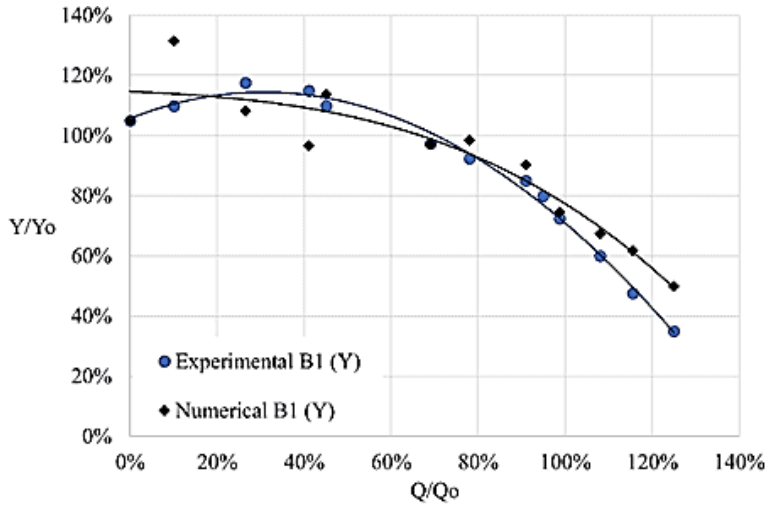

Fig. 15 YxQ curve obtained from the numerical analysis

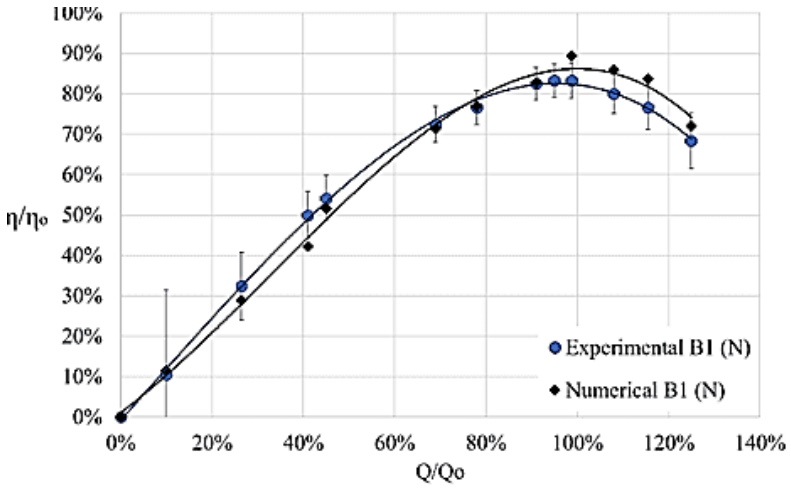

Fig. 16 ηxQ curve obtained from the numerical analysis

Table 5 Pump design parameters

d/D	*U*	*Cm*	*ΔCu*	β∞	*W*∞	$C_l.(l/t)$
m	m/s	m/s	m/s	degree	m/s	-
0	7.72	5.8	3.97	45.2	8.2	0.97
0.125	8.69	5.8	3.53	40	9.0	0.78
0.25	9.65	5.8	3.18	35.7	9.9	0.64
0.375	10.6	5.8	2.9	32.3	10.8	0.53
0.5	11.6	5.8	2.65	29.4	11.8	0.45
0.625	12.6	5.8	2.44	27.0	12.8	0.38
0.75	13.5	5.8	2.27	25.0	13.7	0.33
0.875	14.5	5.8	2.12	23.3	14.7	0.29
1	15.5	5.8	1.99	21.8	15.6	0.25
d/D	*U*	*Cm*	*ΔCu*	β∞	*W*∞	$C_l.(l/t)$

4. CASE STUDY

4.1 Circulating Water Channel and Pump Specification

Table 5 shows the design parameters of the CWC and pump.

Using the dimensioning methodology through the theory of linear cascades together with the criterion of the minimum pressure coefficient, the complete geometry of the pump was defined. To reach the necessary lift coefficient, profiles from the NACA 65 family were selected. This family of profiles was selected because they had their maximum thickness at 40% of the chord and maximum curvature at 50% of the chord. In this way, smoother loading was achieved such that the possibility of cavitation was reduced. Another recommendation considered was that the profiles needed to have a maximum ratio between thickness and chord between 15% and 18% to avoid performance losses (Gülich, 2014).

4.2 Pump Design by the Minimum Pressure Coefficient Criterion

With the initial considerations and after applying the minimum pressure coefficient criterion, the Thoma coefficient was calculated through Eq. 13. *Cpmin* in Table 6 was the reference used as a criterion for the selection of cascade profiles and within the recommended range for the hub profile.

From the pressure distribution limitations defined by the cavitation analysis, the following profiles were

Table 6 *Cpmin* criterion application and cavitation analysis

Diameter	Thoma Coefficient	Reynolds Number	*Cpmin*	*Cpmin* + σ
0.737	3.449	5.35E+06	-1.7	1.749
0.830	2.791	6.75E+06	-1.7	1.090
0.922	2.288	8.35E+06	-1.7	0.590
1.014	1.901	1.02E+07	-1.5	0.401
1.106	1.599	1.22E+07	-1.4	0.199
1.198	1.360	1.44E+07	-1.2	0.160
1.291	1.169	1.69E+07	-1.0	0.169
1.383	1.013	1.96E+07	-0.9	0.113
1.475	0.886	2.25E+07	-0.8	0.086

Table 7 Constructive references

Blade Section	*l* (mm)	*l/t*	C_l	β(°)	α (°)
hub	656	0.850	1.146	49.5	4.22
a	748	0.861	0.909	43.1	3.21
b	841	0.871	0.734	38.5	2.84
c	936	0.882	0.604	34.8	2.55
d	1034	0.893	0.503	31.8	2.35
e	1133	0.903	0.425	28.8	1.72
f	1235	0.914	0.363	26.8	1.68
g	1339	0.924	0.313	24.2	0.82
Tip	1444	0.935	0.273	22	0.25

selected for the initial pump geometry. The initial criterion was selected from Series 65 due to the smoother pressure distribution, and from then on, the chord/pitch ratio that Fernandes (1973) used to design the pump within the acceptable *Cpmin* range served as a reference. The data obtained are listed in Table 7. From the Howell diagram, the solidity value of the stator could be determined (Jaberg, 1999).

The number of stator blades varies from 5 to 8 with a smaller number of blades for smaller pumps. The axial distance between the rotor and stator blades needs to be approximately 5% of the external diameter of the rotor so that it does not affect the performance of the machine (Stepanoff, 1957).

In this design methodology, SolidWorks software was used, and a MATLAB code was implemented to increase the efficiency of the process (Fig.17). The visualization of the pump (Fig. 18) was performed using 3D CAD. The use of this tool enabled the editing and alteration of the drawing without accumulating losses in quality or high additional costs

4.3 CFD Verification

The CFD model for studying the axial-flow pump is the same as that used during the validation, with the difference of the addition of the stator at the rotor outlet. A total of 3 cases of simulation were carried out: Case 1 with the rotor designed at 80% of estimated hydraulic efficiency, Case 2 with the rotor designed at 90% estimated hydraulic efficiency, and Case 3 with the rotor designed at 90% estimated efficiency and the use of a

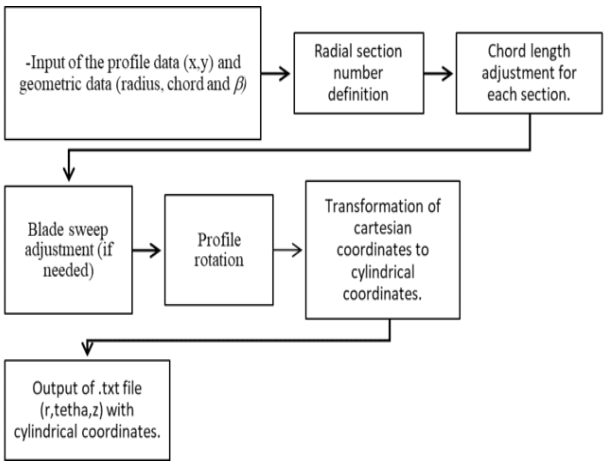

Fig. 17 MATLAB code used

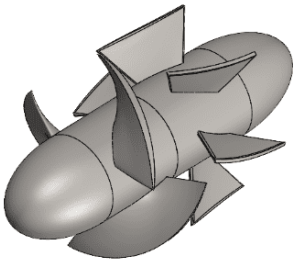

Fig. 18 Pump CAD model

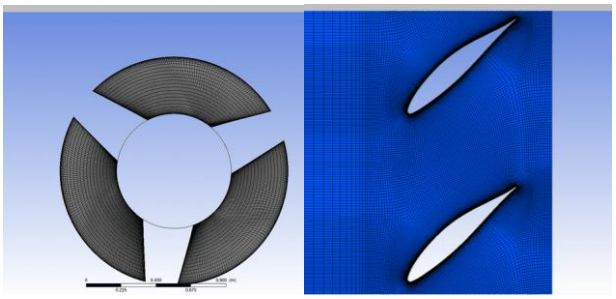

Fig. 19 Pump mesh around the blade surface and profile

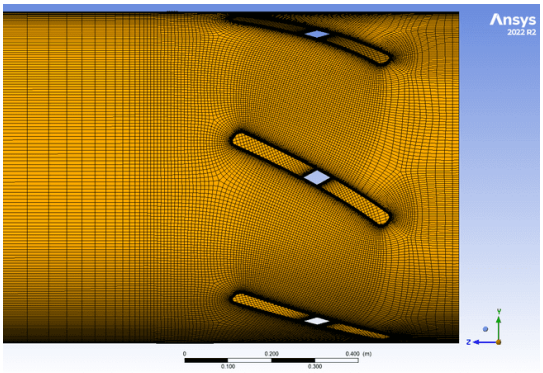

Fig. 20 Mesh at the OGV hub profile

diffuser. In the latter case, a periodicity condition was used, aiming at greater computational efficiency. Figures 19-21 show the refinement of the mesh at the boundary layer of the hub profile and the distribution of the points on its surface.

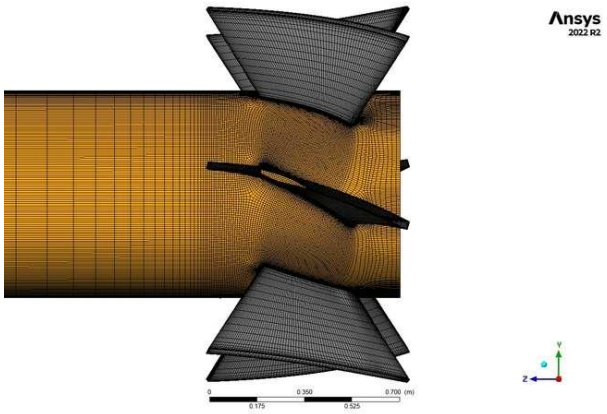

Fig. 21 Mesh at the OGV surface

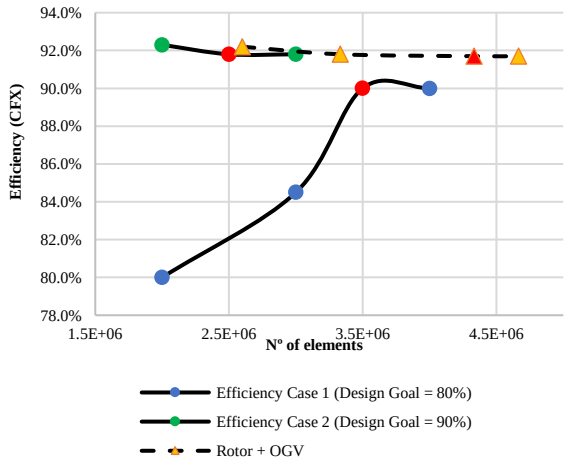

Fig. 22 Mesh independence test for the water channel pump

As the efficiency initially obtained was 12% above the estimated value in the project in Case 1, a new geometry was designed using the same profiles,

Table 8 Mesh independence test for the water channel pump

	Mesh	N° of elements	Efficiency	GCI
Case 1	Mesh 5	2.06E+06	80.0%	-
	Mesh 6	3.15E+06	84.5%	6%
	Mesh 7	3.53E+06	90.0%	7%
	Mesh 8	4.52E+06	90.0%	0%
Case 2	Mesh 9	2.15E+06	92.3%	-
	Mesh 10	2.66E+06	91.8%	1%
	Mesh 11	3.15E+06	91.8%	0%
Case 2 + OGV	Mesh 12	2.67E+06	92.0%	-
	Mesh 13	3.36E+06	91.8%	0%
	Mesh 14	4.34E+06	91.7%	0.1%
	Mesh 15	4.67E+06	91.7%	0.0%

geometrically varying only the solidity, as recommended in the literature. A new simulation was then performed using the new geometry, with 90% of estimated hydraulic efficiency (Case 2). Figure 22 and Table 8 show the mesh convergence study, with the selected mesh for each case marked in red.

The first simulation in this situation served as a support and complement to the cascade dimensioning methodology through an iterative process. For the stator domain convergence analysis, the mesh selected above was coupled with the stator domain, and the stator pressure gain was compared for three situations. This configuration was selected for the machine performance analysis using the *Cpmin* criterion.

In Figure 23, the velocity and pressure field in the 3 radial sections of the hub, midspan and tip of the blade at

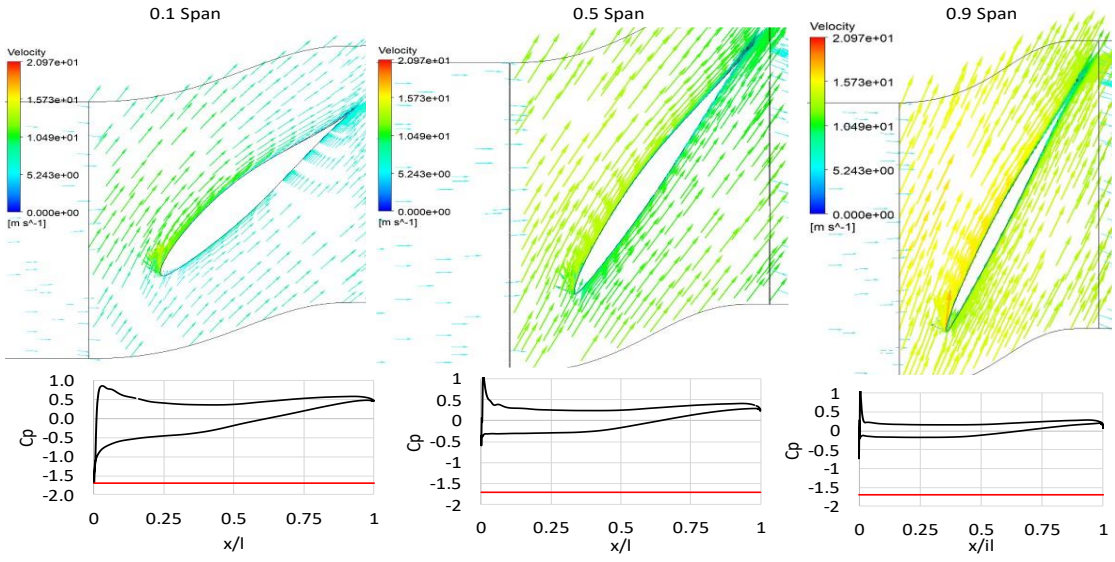

Fig. 23 Pressure and velocity distribution around the hub mid and tip span of the blade at the design flow rate

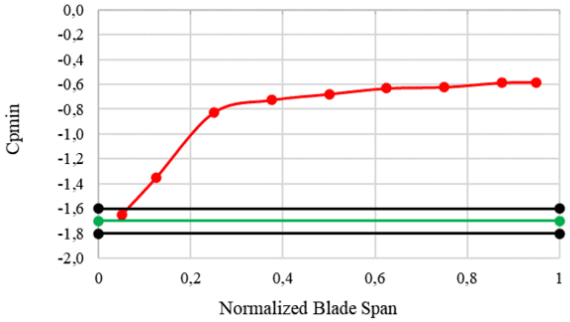

Fig. 24 Pressure distribution throughout the blade span

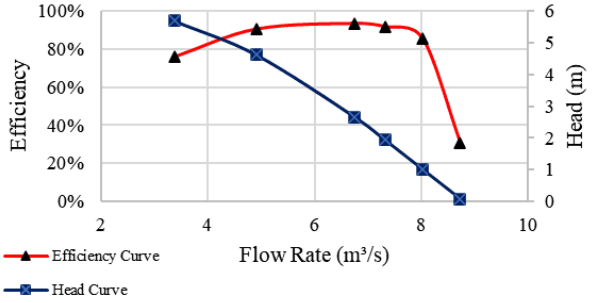

Fig. 25 Characteristic curves of the pump

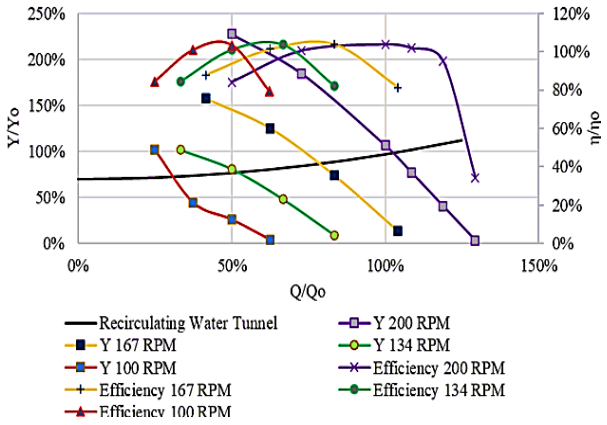

Fig. 26 Characteristic curves of the rotor at variable speeds

the design flow rate for Case 2 is shown. A smooth distribution of the velocity profile was observed. From the velocity field, there was no noticeable flow separation along the blade, and the load was effectively distributed in all sections, which increased the efficiency of the machine and avoided related losses. This confirmed the pressure coefficient criterion as an effective cascade selection criterion.

Figure 24 shows the pump's *Cpmin* distribution. The loading is within the cavitation limits, and the *Cpmin* at the blade root is within the recommended limit.

The pump efficiency and head generated were obtained through CFD calculations. In these curves (Fig. 25), the flows selected for simulation were within the allowable range, and the characteristic unstable region of axial-flow pumps was not reached; these results indicated that within this range, its behavior would be stable.

High efficiency values were obtained for the design flow when η_o was equal to 90%, indicating that the pressure coefficient criterion was a qualified parameter for selecting cascades for axial-flow turbomachines. Figure 26 shows the behavior of the pump operating at variable speed. The values were normalized based on the design flow rate of the pump, which was equivalent to a velocity of 3 m/s in the water channel flow.

5. CONCLUSION

The results obtained through the numerical validation of the experimental tests carried out by Fernandes (1973) showed that the design *Cpmin* value varies according to the variation in the pump operating flow. This causes severe efficiency losses when operating outside the design point.

Pumps designed using the *Cpmin* criterion showed good efficiency at the design point. However, its operation at variable speeds needed attention since the operating point was not in the instability zone of the pump curve. This behavior tended to occur at low speeds.

It was observed through the pump curves that the lower the flow rate (100 RPM for instance), the more the operating point approaches the instability zone. This can be a reason for the drop in performance in low flow rates. A possible solution for this could be an analysis on the flow at the outlet conduit of the pump, together with a better design of the outlet guide vanes, to avoid reverse flow.

By using the criterion of the minimum pressure coefficient within the recommended range, a high efficiency for the axial pump and a flow without flow separation were obtained. The machine efficiency decreased during operation at reduced speed, which was associated with the change in the Cp distribution on the blade, as demonstrated by the validation.

Notably, the efficiency of the machine at the nominal point showed that the criterion could be applied only in the region of greatest loading of the blade without major impacts on its performance. A comparison approach of design methods for large axial pumps is recommended to deepen the understanding of the benefits of the minimum pressure coefficient criterion.

For future works, the impacts of adding vanes at the rotor inlet on its sensitivity to cavitation will be investigated and the optimal way to install the vanes at the rotor outlet to cause the flow in the water channel to be as smooth as possible will be verified. Another design aspect that needs to be further analyzed is the operation at low speed to satisfactorily reach low flow velocities in the test section. Another research avenue is to revise the number of design blades for both the rotor and the stator by increasing the number of blades. With this modification, a reduction in the noise generated by the machines and greater pressure recovery in the stage can potentially be achieved.

ACKNOWLEDGEMENTS

The work presented was supported by the Coordenação de Aperfeiçoamento de Pessoal de Nível Superior – Brasil (CAPES), the Federal University of Pará through the Laboratory of Fluid Dynamic and Particulate and by the Brazilian agency FAPEMIG through the research project APQ-01865-18.

CONFLICT OF INTEREST

There are no conflicts to disclose.

AUTHORS CONTRIBUTION

R. V. Correia Ramalho: Data curation, Investigation, Software, Validation, Visualization, Writing – original draft; **A. L. Amarante Mesquita**: Conceptualization, Resources, Supervision, Writing – review & editing; **N. Manzanares Filho**: Supervision, Writing – review & editing.

REFERENCES

Ahn, J. W., Kim, G. D., Kim, K. S., Lee, J. T., & Seol, H. S., (2008). Development of the driving pump for the low noise large cavitation channel. *Journal of the Society of Naval Architects of Korea*, *45*(4), 370–378. https://doi.org/10.3744/SNAK.2008.45.4.370

Al-Obaidi, A. R. (2019). Investigation of fluid field analysis, characteristics of pressure drop and improvement of heat transfer in three-dimensional circular corrugated pipes. *Journal of Energy Storage*, *26*, 101012. https://doi.org/10.1016/j.est.2019.101012

Amarante Mesquita, A. L., Araújo, A. V., Pacha, R., Souza, J. M. R., & Tachibana, T. (2015). River school boat for safely transporting students in Portuguese. *Proceedings of the 24th Pan-American Conference of Naval Engineering, Maritime Transport and Port Engineering*, Copinaval, Montevideo, Uruguay, October.

Amarante Mesquita, A. L., Cruz, D. O. A., Serra, C. M. V., & Manzanares Filho, N. (1999). A simplified method for axial-flow turbomachinery design. *Journal of the brazilian society of mechanical sciences and engineering*, *21*(1), 61-70.

ANSYS TurboGrid Tutorials. (2015). *ANSYS TurboGrid.* ANSYS, Inc. Canonsburg, PA 15317 USA.

Assi, G. R. S., Meneghini, J. R., Aranha, J. A. P., Coleto, W. G. (2005). *Design, assembling and verification of a circulating Water channel facility for fluid dynamics experiments.* 18th International Congress of Mechanical Engineering, Ouro Preto, MG, Brazil. https://www.abcm.org.br/anais/cobem/2005/PDF/COBEM2005-1238.pdf

Castegnaro, S. (2018). Aerodynamic design of low-speed axial-flow fans: A historical overview. *Designs*, 2(3), 1–17. https://doi.org/10.3390/designs2030020

Choi, J. K., Kim, H. T., Lee, C. S., & Lee, S. J. (2021). A numerical study on axial pump performance for large cavitation channel operation, *Processes*, *9*, 1523. https://doi.org/10.3390/pr9091523

Cruz, A. G. B., Amarante Mesquita, A. L., & Blanco, C. J. C. (2008). Minimum pressure coefficient criterion applied in axial-flow hydraulic turbines, *Journal of the Brazilian Society of Mechanical Sciences and Engineering*, *30*(1), 30-38. https://doi.org/10.1590/S1678-58782008000100005

Denton, J. D. (2010). *Some limitations of turbomachinery CFD.* ASME Turbo Expo, Glasgow, UK.

Dönmez, A. H., Yumurtacı, Z., & Kavurmacıoğlu, L. (2023). Influence of inlet vane and wrap angles on cavitation behavior of a centrifugal pump. *Journal of Applied Fluid Mechanics*, *16*(3), 519–531. https://doi.org/10.47176/jafm.16.03.1342.

Drela, M. (June 5-7). *XFOIL: An analysis and design system for low Reynolds number airfoils.* In Low Reynolds Number Aerodynamics: Proceedings of the Conference Notre Dame, Indiana, USA, Springer Berlin Heidelberg. https://doi.org/10.1007/978-3-642-84010-4_1

Fernandes, E. C. (1973). *Analysis of the geometric parameter influences on the axial-flow turbomachine design, in Portuguese*. [Master's thesis, *Technologic Institute of Aeronautic*]. São José dos Campos.

Grinberg, M., Padovezi, C. D., & Tachibana, T. (2011). *Use of Small Scale Model Tests to define optimized ship shapes.* XXII Copinaval – IPIN, Buenos Aires.

Gucheng, Z., Zuogang, C., & Yi, D. (2021). A numerical investigation on hydrodynamic characteristics of the circulating water channel. *Ocean Engineering*, *236*, 109564. https://doi.org/10.1016/j.oceaneng.2021.109564

Gülich J. F. (2014). Pump types and performance data. *Centrifugal*, 43-78. https://doi.org/10.1007/978-3-642-40114-5

Guo, B., Wang, D., Zhou, J., Shi, W., & Zhou, X. (2020). Performance evaluation of a submerged tidal energy device with a single mooring line. *Ocean Engineering*, *196*, 106791. https://doi.org/10.1016/j.oceaneng.2019.106791

Haghighi, M. H. S., Mirghavami, S. F., Chini, S. M., & Riasi, A. (2019). Developing a method to design and simulation of a very low head axial turbine with adjustable rotor blades, *Renew Energy*, *135*, 266-276. https://doi.org/10.1016/j.renene.2018.12.024

Holanda, P. S., Blanco, C. J. C., Amarante Mesquita, A. L., Brasil Junior, A. C. P., Figueiredo, N. M., Macêdo, E. N., & Secretan, Y. (2017). Assessment of hydrokinetic energy resources downstream of hydropower plants, *Renew Energy*, *101*, 1203–14. https://doi.org/10.1016/j.renene.2016.10.011

Hosono, K., Kajie, Y., Saito, S., & Miyagawa, K. (2015). Study on cavitation influence for pump head in an axial flow pump. *Journal of Physics: Conference Series*,

Publishing. https://doi.org/10.1088/1742-6596/656/1/012062

Jaberg, H. (1999). *Hydraulic aspects in design and operation of axial flow pumps*. Institute for Hydraulic Machinery, Graz, Austria. S. https://doi.org/10.1007/978-3-642-40032-2

Martinez, R., Ordonez Sanchez, S., Allmark, M., Lloyd, C., O'Doherty, T., Germain, G., Gaurier, B., & Johnstone, C. (2020). Analysis of the effects of control strategies and wave climates on the loading and performance of a laboratory scale horizontal axis tidal turbine, *Ocean Engineering*, *212*, 107713. https://doi.org/10.1016/j.oceaneng.2020.107713

Menter, F. R., Matyushenko, A., & Lechner, R. (2020). Development of a generalized k-ω two-eq. turbulence model. *New Results in Numerical and Experimental Fluid Mechanics XII*, 101–109. https://doi.org/10.1007/978-3-030-25253-3_10

Menter, F. R. (1993). *Zonal two Eq. k-ω turbulence models for aerodynamic flows.* 24th fluid dynamics conference, Orlando, Florida. https://ntrs.nasa.gov/citations/19960044572

Muis, A., Sutikno, P., Soewono A., & Hartono, F. (2015). Design Optimization of Axial Hydraulic Turbine for Very Low Head Application, *Energy Procedia*, *68*, 263-273. https://doi.org/10.1016/j.egypro.2015.03.255

Nguyen, D. A., Ma, S. B., Kim, S., & Kim, J. H. (2023). Hydrodynamic optimization of the impeller and diffuser vane of an axial-flow pump. *Journal of Mechanical Science and Technology* https://doi.org/10.1007/s12206-022-1217-0

Pfleiderer, C., & Petermann, H. (1979). *Flow Machines*. Technical and Scientific Books S/A. Rio de Janeiro, RJ, Brazil. https://doi.org/10.1007/b138287

Pinto, R. N., Afzal, A., D'Souza, L. V., Ansari, Z., & Samee, A. D. M. (2017). Computational fluid dynamics in turbomachinery: A review of state of the art. *Arch Computational Methods Eng*, *24*, 467–479. https://doi.org/10.1007/s11831-016-9175-2

Schlichting, H., & Truckenbrodt, E. (1959) *Aerodynamik des Flugzeuges*. Berlin: Springer-Verlag. https://doi.org/10.1007/BF00536536

Scholz, N. (1965). Aerodinamik der Scaufelgitter. In I. Band G. Verlag (Eds.), *Braun, Karlsruhe*.

Shi, L. J., Tang, F. P., Liu, C., Xie, R. S., & Zhang, W. P. (2016). Optimal design of multi-conditions for axial flow pump. *Earth and Environmental Science*, *49*. https://doi.org/10.1088/1755-1315/49/6/062028

Silva, P. A. S. F., Shinomiya, L. D., Oliveira, T. F., Vaz, J. R. P., Amarante Mesquita, A. L., & Brasil Junior, A. C. P. (2017). Analysis of cavitation for the optimized design of hydrokinetic turbines using BEM. *Applied Energy*, *185*, 1281-1291. https://doi.org/10.1016/j.apenergy.2016.02.098

Srinivasan, K. M. (2008). *Rotodynamic pumps (Centrifugal and axial).* New Age International Publishers.

Stepanoff, A. F. (1957). *Centrifugal ad axial flow pumps: Theory, Design and application*, 2n ed. Wiley, NY. https://doi.org/10.1007/978-3-662-25101-0

Stephen, C. K. (1971). *Design and construction of a water channel.* National Science Foundation Project.

Sutikno, P., & Adam. I. K. (2011). Design, simulation and experimental of the very low head turbine with minimum pressure and free vortex criterions, *International Journal of Mechanical and Mechatronics Engineering*, *11*(1), 9-15. https://www.ijens.org/Vol%2011%20I%2001/113701-2828%20IJMME-IJENS.pdf

Tyacke, J., Vadlamani, N. R., Trojak, W., Watson, R., Ma, Y., & Tucker, P. G. (2019). Turbomachinery simulation challenges and the future. *Progress in Aerospace Sciences*, *110*, 100554. https://doi.org/10.1016/j.paerosci.2019.100554

Wang, Z., Cheng, H., Bensow, R. E., Peng, X., & Ji, B. (2023). Numerical assessment of cavitation erosion risk on the Delft twisted hydrofoil using a hybrid Eulerian-Lagrangian strategy. *International Journal of Mechanical Sciences*, *259*, 108618, https://doi.org/https://doi.org/10.1016/j.ijmecsci.2023.108618

Watanabe, T., Sato, H., Henmi, Y., Horiguchi, H., Kawata, Y., & Tsujimoto, Y. (2009). Rotating choke and choked surge in an axial pump impeller. *International Journal of Fluid Machinery and Systems*. *2*(3), 232–238. https://doi.org/10.5293/IJFMS.2009.2.3.232

Wilcox, D. C. (2006). *Turbulence Modeling for CFD*. 3rd edition, DCW Industries, Inc., La Canada CA.

Wu, C. H. (1952). *A general theory of steady three-dimensional flow of a non-viscous fluid in Subsonic and Supersonic Turbomachines of Axial-, Radial, and Mixed-Flow Types.* NACA, Washington. http://hdl.handle.net/2060/19930083325

Xie, C., Zhang, C., Fu, T., Zhang, T., Feng, A., & Jin, Y. X. (2019). Numerical analysis and model test verification of energy and cavitation characteristics of axial flow pumps. *Water*, *14*(18), 2853. https://doi.org/10.3390/w14182853.

Ye, J., Tan, L., Shi, W., Chen, C., & Francis, E. M. (2022). Numerical simulation of axial-flow pump cavitation based on variable frequency speed regulation. *Water*, *14*(17). https://doi.org/10.3390/w14172757.

Zhang, Y., Najafi, M. J., Heydari Beni, M. H., Davar, A., Toghraie, D., Shafiee, B. M., Jam, J. E., & Hekmatifar, M. (2022). The effects of geometric shapes at different assembly gaps to achieve the optimal hydrodynamic conditions. *Renew Energy*, *184*, 452-459. https://doi.org/10.1016/j.renene.2021.11.099